

Probabilistic Shaping for High-Speed Unamplified IM/DD Systems with an O-Band EML

Md Sabbir-Bin Hossain, *Graduate Student Member, IEEE*, Georg Böcherer, *Member, IEEE*, Talha Rahman, *Member, IEEE*, Tom Wettlin, Nebojša Stojanović, *Member, IEEE*, Stefano Calabrò, and Stephan Pachnicke, *Senior Member, IEEE*

Abstract—Probabilistic constellation shaping has been used in long-haul optically amplified coherent systems for its capability to approach the Shannon limit and realize fine rate granularity. The availability of high-bandwidth optical-electronic components and the previously mentioned advantages have invigorated researchers to explore probabilistic shaping (PS) in intensity-modulation and direct-detection (IM/DD) systems. This article presents an extensive comparison of uniform 8-ary pulse amplitude modulation (PAM) with PS PAM-8 using cap and cup Maxwell-Boltzmann (MB) distributions as well as MB distributions of different Gaussian orders. We report that in the presence of linear equalization, PS-PAM-8 outperforms uniform PAM-8 in terms of bit error ratio, achievable information rate and operational net bit rate indicating that cap-shaped PS-PAM-8 shows high tolerance against nonlinearities. In this paper, we have focused our investigations on O-band electro-absorption modulated laser unamplified IM/DD systems, which are operated close to the zero dispersion wavelength.

Index Terms—IM/DD, Probabilistic shaping, Maxwell-Boltzmann, pulse-amplitude modulation, Volterra nonlinear equalizer, forward error correction, achievable information rate.

I. INTRODUCTION

COMMUNICATION channel models like the additive white Gaussian noise (AWGN) channel often have non-uniform capacity-achieving input distributions. This has been the main motivation for probabilistic shaping (PS), i.e., the development of practical transmission schemes that use non-uniform distributions at the input of the channel. Many different PS schemes have been proposed in literature, see, e.g., the literature review in [1, Sec. II].

An important milestone for making PS practical was the invention of probabilistic amplitude shaping (PAS) [1], which concatenates a shaping outer code called a distribution matcher [2] and a forward error correction (FEC) inner code.

Manuscript received 8 February 2023; revised 13 March 2023; accepted 24 March 2023. Date of publication XX XXXX 2023; date of current version XX XXXX 2023. The author(s) received no specific funding for this work. (corresponding author: Md Sabbir-Bin Hossain)

Md Sabbir-Bin Hossain is with Kiel University (CAU), Chair of Communications, Kaiserstr. 2, 24143 Kiel, Germany and with Huawei Munich Research Center, Riesstr. 25, 80992 Munich, Germany (e-mail: sabbir.hossain@huawei.com).

Georg Böcherer, Talha Rahman, Tom Wettlin, Nebojša Stojanović, and Stefano Calabrò are with Huawei Munich Research Center, Riesstr. 25, 80992 Munich, Germany (e-mail: {georg.bocherer, talha.rahman, tom.jonas.wettlin, nebojsa.stojanovic, stefano.calabro}@huawei.com).

Stephan Pachnicke is with Kiel University (CAU), Chair of Communications, Kaiserstr. 2, 24143 Kiel, Germany (e-mail: stephan.pachnicke@tf.uni-kiel.de).

The PAS architecture has three properties that distinguish it from other proposed PS schemes. First, it integrates PS with existing FEC, second, it achieves the Shannon limit [3, Sec. 10.3], third, it supports configurability of the PS overhead (OH) by changing the probability distribution. This additional degree of freedom is beneficial for transceiver design. For instance, supposing that net bit rate, modulation format, and FEC OH are fixed and given, we can still optimize a PAS design by trading PS OH against baud rate. Because of these three properties, PAS plays an important role in coherent optical transmission systems [4] and state-of-the-art transceivers implement PAS, see, for instance, [5]–[7].

However, until today, for short-reach applications (up to 5 km), intensity-modulation with direct-detection (IM/DD) is preferred over coherent transmission [8], [9]. Recent studies show progress towards 400 Gb/s/lane [10]–[12], which leverage the early availability of high bandwidth (BW) optoelectronic (OE) components. In this context, shaping gain and configurable PS OH make PAS potentially attractive also for IM/DD systems [13]–[17].

The Maxwell-Boltzmann (MB) distribution, which is close to the optimum distribution for Gaussian channels [18], minimizes the average power for a given source entropy. Since coherent systems typically contain optical amplifiers and are subject to an average power constraint (APC), they benefit from the MB distribution. However, typical IM/DD systems do not use optical amplification and, therefore, are considered unamplified in this work (at high symbol rates IM/DD systems might require optical amplification). Unamplified IM/DD systems are often considered as peak-power constrained (PPC). Under the idealized assumption that the modulator transfer function has a sharp transition from the linear region to the saturation, it was shown that the cup (reverse) MB distribution is beneficial and a shaping gain up to 0.47 dB was demonstrated numerically for PAM-4 [16]. A comprehensive study of probabilistic shaping (PS) for unamplified IM/DD was presented in [17], where both unipolar and bipolar MB and reverse MB distributions are investigated. The key insight of [17] for unamplified IM/DD is as follows. If the system is PPC, PS does not bring much gain. On the other hand, if the peak-to-average power ratio (PAPR) is already very large, e.g., due to bandlimited components, then considerable PS gains can be observed.

In reality, the modulator transfer function shows a relatively slow transition from the linear to the nonlinear region. This results in a new scenario in unamplified IM/DD systems,

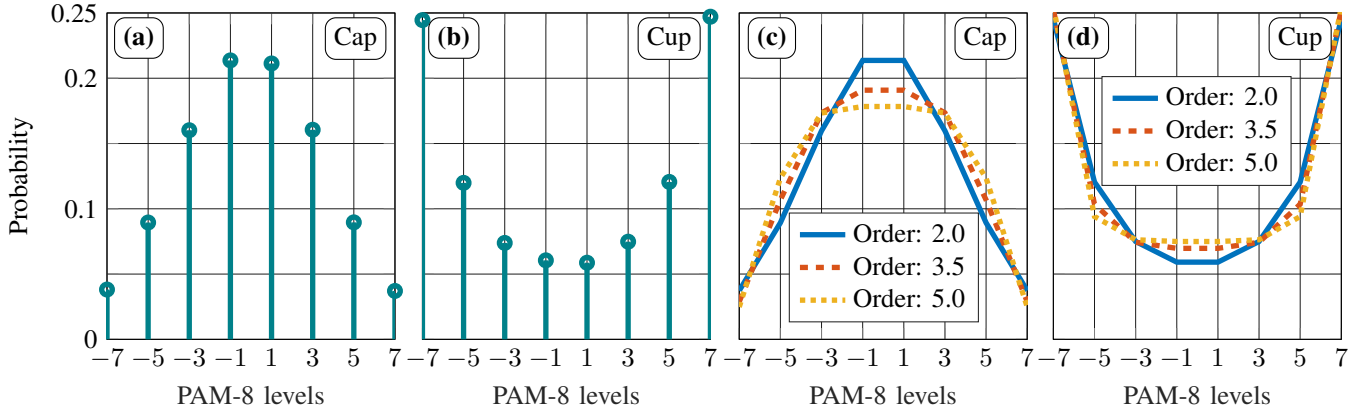


Fig. 1: PS PAM-8 symbol distribution: (a) and (b) show the cap and cup-shaped variants of the MB distribution, respectively. Modified MB distributions with different Gaussian orders are shown for both cap and cup variants in (c) and (d), respectively.

which lies somewhere in between PPC and APC systems. In this paper, we discuss how to exploit the characteristics of an electro-absorption modulated laser (EML) by optimizing the driving voltage both for 8-ary uniform and PS pulse-amplitude modulation (PAM).

This paper, which is supported by experimental demonstration with an unamplified IM/DD system, is a follow-up on our recently published works [13]–[15] and presents theoretical and physical reasoning on the performance of multiple variants of the MB distribution.

The remainder of the paper is structured as follows. In Section II, PS is discussed for cap (MB distribution) and cup-shaped (reverse MB distribution) variants with different Gaussian orders (GOs). Afterward, driving voltage optimization and its performance are described in Section III. Sections IV and V describe the experimental setups used for evaluating uniform and PS PAM-8 and present experimental results with discussions, respectively. Section VI concludes the paper.

II. PROBABILISTIC AMPLITUDE SHAPING FOR IM/DD SYSTEMS

PAS [1] concatenates at the transmitter side a distribution matcher (DM) [2] with an off-the-shelf systematic FEC encoder. The DM imposes the desired distribution on the shaped bits, while the FEC encoder generates additional parity bits. As no specific distribution can be imposed on the parity bits, they must be treated as uniformly distributed.

A. PAS for Coherent Transmission

Coherent systems with optical amplification operate subject to an average power constraint. In this case the squared amplitude of a symbol from the amplitude shift keying (ASK) constellation

$$\mathcal{X}_{\text{ASK}} = \{\pm 1, \pm 3, \dots, \pm(2^m - 1)\} \quad (1)$$

acts as the cost of the symbol. Consequently, PAS maps the shaped bits to amplitudes and imposes a distribution that minimizes the average power. The parity bits are mapped to signs, as the average power is invariant under the distribution

of the signs. The distribution that minimizes the average power is an MB distribution given by

$$P_{\text{MB}}^{\nu}(x) \propto e^{-\nu|x|^2}, \quad \nu \geq 0, x \in \mathcal{X}_{\text{ASK}}. \quad (2)$$

The parameter ν controls the degree of shaping, i.e., for $\nu = 0$, X is uniformly distributed, while for ν large, the probability of the outer symbols approaches zero.

B. PAS System Parameters [19]

For 2^m -ASK constellations, there are $m - 1$ amplitude bits and 1 sign bit, so the FEC rate must be at least $\frac{m-1}{m}$, since otherwise, the FEC encoder would produce more than 1 parity bit per ASK symbol. Correspondingly, the FEC OH must be smaller than $\frac{1}{m-1}$. For instance, for 16-QAM, corresponding to 4-ASK in each real tributary, the FEC OH can be at most 100%, while for 64-QAM, the FEC OH can be at most 50%. FEC OHs of practical systems are smaller, so the OH constraint plays no further role in practice.

By [19], the spectral efficiency of PAS with an ideal DM is

$$\text{SE} = [\text{H}(X) - m(1 - R_{\text{FEC}})]^+ \quad (3)$$

where $\text{H}(X)$ is the entropy of the input in bits and where $[\cdot]^+ = \max\{0, \cdot\}$ ensures the non-negativity of SE.

By [19], [20, Table 1], the PS redundancy is $1 - \frac{\text{H}(X)}{m}$ and the PS OH is

$$\text{PS}_{\text{OH}} = \frac{m}{\text{H}(X)} - 1. \quad (4)$$

FEC and PS redundancy add up, so that the total OH is $\frac{1}{R_{\text{FEC}} + \frac{\text{H}(X)}{m} - 1} - 1$.

C. PAS for Square-Law Detection

The work [21] focuses on the square-law detection by a photodiode (PD) and assumes receiver AWGN added after the PD. In this case, entropy subject to an average power constraint after the PD is maximized by an exponential distribution before the PD. For the exponential distribution, PAS cannot be applied directly. In [22], a pragmatic approach is proposed by assigning the same exponential distribution to the signal points

with odd and even index, respectively. Choosing between odd and even now plays the role of choosing the sign, and PAS can be applied.

D. PAS for IM/DD

In this work, we consider IM/DD without optical amplification and we aim to choose an input distribution suitable for the EML transfer curve, see Fig. 2. We choose a PAM constellation equal to the ASK constellation in (1), i.e.,

$$\mathcal{X}_{\text{PAM}} = \{\pm 1, \pm 3, \dots, \pm(2^m - 1)\} \quad (5)$$

and we consider a more general family of MB distributions

$$P_{\text{MB}}^{\nu, \alpha}(x) \propto e^{-\nu|x|^\alpha}, \quad x \in \mathcal{X}_{\text{PAM}} \quad (6)$$

where α chooses the Gaussian order. The cost associated with symbol x is now $\text{sign}(\nu)|x|^\alpha$ and determined by the symbol amplitude so that when using the PAM constellation (5), the sign does not influence the average cost and PAS can be applied directly.

1) *Cap and Cup MB Distribution:* We set the Gaussian order to the common value $\alpha = 2$. For cap-shaped distributions (Fig. 1(a)) ν is positive, i.e., the exponent is negative. Similarly, for cup-shaped MB distributions (Fig. 1(b)), ν is negative, i.e., the exponent is positive. As expected, both cap and cup MB distributions are symmetric around zero and, therefore, compatible with PAS. The entropy of the cap and cup MB distributions can be set to the desired value by choosing $|\nu|$ accordingly, where a larger $|\nu|$ corresponds to a lower entropy. For each PS OH, there are only one possible cap-shaped and cup-shaped MB distribution, respectively.

2) *Different Gaussian Orders:* We now vary the Gaussian order (GO) α [15]. A similar concept has been introduced in [23] and resulted in super-Gaussian distributions for coherent systems. For each OH, we now have several candidate distributions depending on the order α . The modification applies equally for the cap and cup-shaped variants.

The distributions with GO 2.0, 3.5 and 5.0 for cap and cup-shaped variants in the PAM-8 case are presented in Figs. 1(c) and (d), respectively. As the GO increases from 2.0, corresponding to the classic MB distribution, to GO 5.0, the symbol occurrence of the center PAM levels becomes more uniform and the transition towards the probability of the outer PAM levels becomes sharper.

III. DRIVING VOLTAGE OPTIMIZATION

In this section, we discuss the optimization of the peak-to-peak analog voltage (V_{pp}) as driving voltage of the modulator. As we show in the following, this parameter controls the trade-off between extinction ratio (ER) and modulator nonlinearity and affects the choice of the shaping distribution.

In our investigation we consider an EML operating near the zero-dispersion wavelength (1310.9 nm) [11], [12]. The transfer curve of the EML, which is used in the experiment, is shown in Fig. 2, where we represent the EML output power as a function of the bias voltage. The operation bias point is generally chosen approximately in the inflection point of the transfer curve to utilize homogeneously the upper and lower

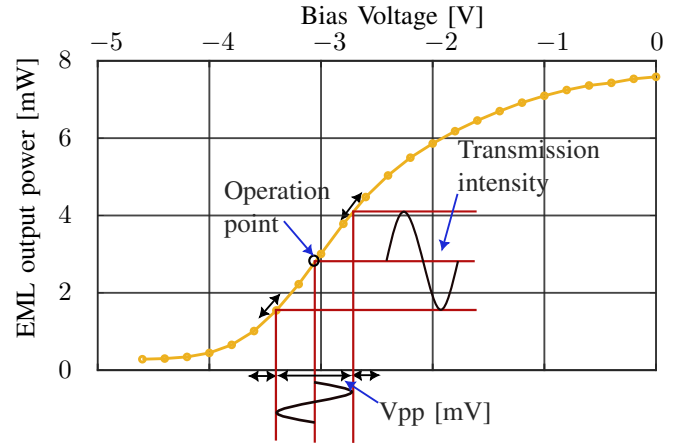


Fig. 2: EML transfer curve (measured) with exemplary modulation of a sine wave signal.

portion of the transfer curve. For this particular scenario, the considered EML would be operated at the bias voltage of -3.1 V.

The EML transfer function can be expressed as [24]

$$H_{\text{EML}} = |\sqrt{1 + \beta^2} \cos(\theta + \arctan \beta)|. \quad (7)$$

Here β is the chirp parameter of the EML, which describes the relationship between intensity modulation and phase modulation. β varies with the bias voltage: A larger negative value of β is expected for larger negative bias voltages and vice-versa [24]. The EML transfer curve has two distinctive features:

- It shows a slow transition from the linear to the nonlinear region.
- Its chirp (β) varies with the bias voltage.

Fig. 2 illustrates the modulation of a sine wave. The EML is biased approximately in the inflection point of the linear region. By regulating the driving voltage we can control the ER and the used nonlinear region of the EML transfer curve. The optimum driving voltage highly depends on the modulation format and the symbol occurrence probability. As shown in Fig. 1, with the cup-shaped MB distribution, the outer levels have higher occurrence probability and, therefore, are affected by distortion which leads to higher noise variance. For the cup distribution, the optimum V_{pp} is generally lower in comparison to both cap-shaped and uniform PAM-8. The cap distribution has the lowest symbol occurrence on the outer levels and tolerates a high V_{pp} without suffering from nonlinear distortions. Therefore, the cap-shaped distribution allows for ER enhancement, which leads to better separation between neighboring levels and improves the bit error ratio (BER) performance. For uniform PAM-8, the optimum V_{pp} is in between the optimal values for cap and cup-shaped distributions.

Chirp dependence on bias voltage also plays an important role when fiber transmission is performed for the comparison between uniform and PS PAM-8. As explained, higher negative and lower negative bias voltages result in high negative and positive β values, respectively. The variation of the β

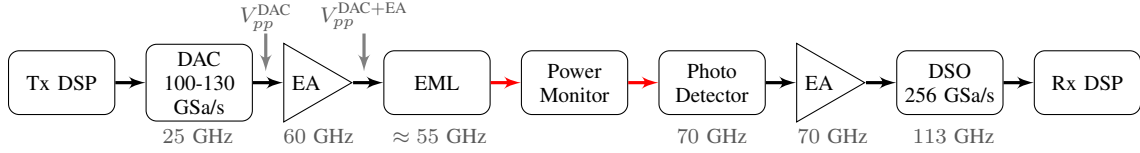


Fig. 3: Schematic of the IM/DD transmission system used for the experimental investigations. DAC: digital-to-analog converter, EA: electrical amplifier, EML: electro-absorption modulated laser, DSO: digital storage oscilloscope.

values results in nonlinear distortions. For the cap variant, most of the symbols are transmitted around the zero level, where $|\beta|$ is smaller, which reduces the impact of nonlinear distortion. Conversely, the cup variant is more susceptible to nonlinear distortion since most symbols are modulated on the outer levels where $|\beta|$ is higher. Uniform PAM-8 is expected to have an intermediate behavior.

In summary, for an EML, the cap-shaped distribution exhibits two distinct beneficial features:

- $V_{pp} \uparrow \Rightarrow ER \uparrow \Rightarrow$ separation between neighboring levels $\uparrow \Rightarrow BER \downarrow$.
- Most symbol are modulated around the zero level, where $|\beta|$ is not significant \Rightarrow nonlinear distortion \downarrow (only valid when transmission is performed over dispersive fiber link).

IV. EXPERIMENTAL SETUP AND TRANSCEIVER DSP

In this section, the experimental setup and the digital signal processing (DSP) used for experimental evaluation are introduced.

Fig. 3 depicts the optically unamplified IM/DD setup, which is utilized for experimental evaluations. Below each OE component, its 3-dB BW is indicated. Both the transmitter (Tx) and receiver (Rx) side use offline DSP. The block diagrams of the Tx and Rx DSP stacks are shown in Fig. 4. For the transmitter side, a pseudo-random binary sequence (PRBS) is generated and mapped on the uniform PAM-8 levels. Alternatively, for PS-PAM-8, pseudo-random symbols are drawn from an MB distribution with the desired entropy and GO. For uniform PAM-8, the symbol rate is varied from 100 GBd to 130 GBd in 5 GBd steps. For both cap-shaped (Fig. 1 (a)) and cup-shaped (Fig. 1 (b)) distributions, a PS OH (Eq. 4) of $\approx 8.17\%$ is kept constant throughout the experiments. For the cap-shaped (Fig. 1 (c)) variant, GOs of 2.0, 3.5 and 5.0 are used and symbol rates of 110 GBd, 120 GBd and 130 GBd are transmitted. In case of the cup-shaped MB distribution, only a GO of 2.0 at 110 GBd is evaluated.

The mapped symbols are quantized and fed to the digital-to-analog converter (DAC), which is operated at 1 sample per symbol (sps) and has a 3-dB bandwidth (BW) of 25 GHz (6-dB BW ≈ 40 GHz). By changing the frequency of its clock source, the sampling rate of the DAC is varied from 100 to 130 GSa/s. Additionally, we can also vary the voltage swing of the DAC, which we define as V_{pp}^{DAC} in mV unit. After the DAC, an electrical amplifier (EA) of 60 GHz BW with 22 dB gain is used. The resultant amplified electrical output voltage is controlled with the V_{pp}^{DAC} and the output voltage of the DAC and EA, which is also the driving voltage of the modulator,

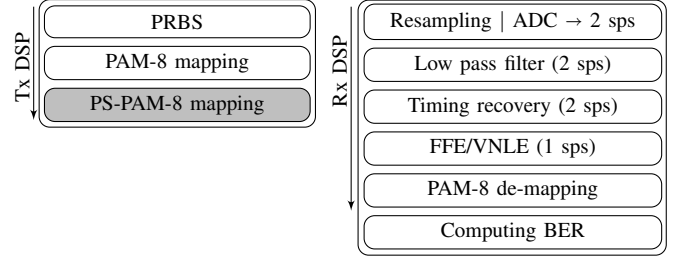


Fig. 4: Block diagram of the offline DSP stack.

is defined as V_{pp}^{DAC+EA} . In Practice, it is difficult to measure the effective V_{pp}^{DAC+EA} . Since the estimation of V_{pp}^{DAC+EA} is dubious, while V_{pp}^{DAC} is known and regulated by us during the experiments, throughout the paper, we report our results w.r.t. V_{pp}^{DAC} . The amplified signal with V_{pp}^{DAC+EA} is then modulated with an O-band EML (3-dB BW ≈ 55 GHz), whose transfer curve is presented in Fig. 2. During the experiments, a current of 66 mA is supplied to the integrated laser diode of the EML and a temperature of $\approx 25^\circ\text{C}$ is maintained for the packaged EML. The EML bias voltage is set to -3.1 V, which leads to an EML output power of ≈ 2.8 mW (4.5 dBm). The driving voltage is regulated via the analog gain of the DAC. At high values of V_{pp} , the nonlinear compression of the modulator can affect the average output power by up to ± 0.1 dBm. Since the variation is not significant, for simplicity, the EML output power is considered ≈ 4.5 dBm independent of the driving voltage. An optional inline power monitor is inserted to measure the output power of the EML, which is also the received optical power (ROP) impinging the 70-GHz PIN PD.

At the receiver, the optical signal is detected and converted to an electrical signal by the PIN PD. Since a proper trans-impedance amplifier was unavailable during the experiments, the electrical signal was amplified with a 70 GHz 11 dB fixed gain EA. The resulting electrical signal is captured with a digital storage oscilloscope (DSO), which operates at 256 GSa/s and has a 3-dB BW of 113 GHz.

For offline processing, 4 million samples are used. The captured samples are first resampled to 2 sps according to the transmission symbol rate. Afterwards, the received signal is normalized by removing the DC components in the signal. Later a low-pass filter designed as finite impulse response filter with filter order 30 is applied to cut the out-of-band noise and prevent aliasing. To estimate and compensate jitter and sampling frequency offset, timing recovery is performed [25]. Either linear feed-forward equalization (FFE) or Volterra nonlinear equalization (VNLE) is performed on every other

symbol (1 sps). In both cases, 301 linear equalizer taps are used to minimize the effect of reflections from the discrete component setup, long copper cables and connectors. For the DSP configuration with VNLE, besides the linear filter taps, additionally 2nd and 3rd order Volterra kernels are used with memory lengths of 7 and 9 symbols to compensate for nonlinearity introduced by DAC, EA, EML and square-law detection, respectively. After equalization (FFE/VNLE), the PAM-8 symbols are de-mapped assuming Gray mapping and the BER is computed.

V. EXPERIMENTAL RESULT AND DISCUSSION

An experimental comparison of uniform PAM-8 and PS PAM-8 with different GOs is presented in this section. The adopted performance metric is pre-FEC BER. Later we interpret the BER result as achievable information rate (AIR) and operational net bit rate (ONBR).

A. Comparison between Uniform and PS PAM-8

The optimization of the driving voltage has been discussed in Section III. Now experimental results for uniform PAM-8, and cap and cup-shaped PS PAM-8 with GO 2.0 are presented in Fig. 5 in the form of pre-FEC BER as a function of V_{pp}^{DAC} . The plot compares 100 GBd uniform PAM-8 with cap and cup-shaped variants (with GO 2.0) with a symbol rate of 110 GBd and PS OH of $\approx 8.17\%$. Considering an HD-FEC with 7% OH (BER threshold of 4.6×10^{-3} [26]), the three formats achieve a similar net bit rate (NBR) of ≈ 280 Gb/s (the NBR for uniform and PS PAM-8 is 280.37 Gb/s and 283.48 Gb/s, respectively).

Fig. 5 presents results obtained with linear (solid lines) and nonlinear (dashed-dotted lines) equalization. For the DSP with FFE only, uniform PAM-8 achieves the lowest BER 1.3×10^{-2} at 260 mV. While the cup-shaped (purple color, square markers) MB variant performs the worst and corresponds to an optimum V_{pp}^{DAC} of 230 mV. Conversely, the cap-shaped (blue color, circle markers) MB variant performs the best with BER improved by more than 7 times compared to uniform PAM-8 at the optimum V_{pp}^{DAC} of 290 mV. As expected, uniform PAM-8 (green color, diamond markers) performs at an intermediate level with the optimum V_{pp}^{DAC} at exactly halfway between the two PS formats. In the presence of VNLE, the performance of all compared schemes is improved. Also, the optimum driving voltage increases significantly in the presence of VNLE. A significant BER improvement is achieved in case of uniform PAM-8 (more than 7 times), while for the cup and cap-shaped distributions, the improvement factor reaches 3 times at most.

Histograms of uniform and PS PAM-8 at their respective optimum V_{pp}^{DAC} after equalization are presented in Fig. 6. Line color and style are kept the same as in Fig. 5. For the cap-shaped PS variant, the linear FFE results in a very distinct level separation, while VNLE compensates the minor nonlinear distortions. For the cup-shaped MB distribution, the VNLE is essential to correct the significant nonlinear distortions. In case of uniform PAM-8, all levels exhibit a reasonable separation

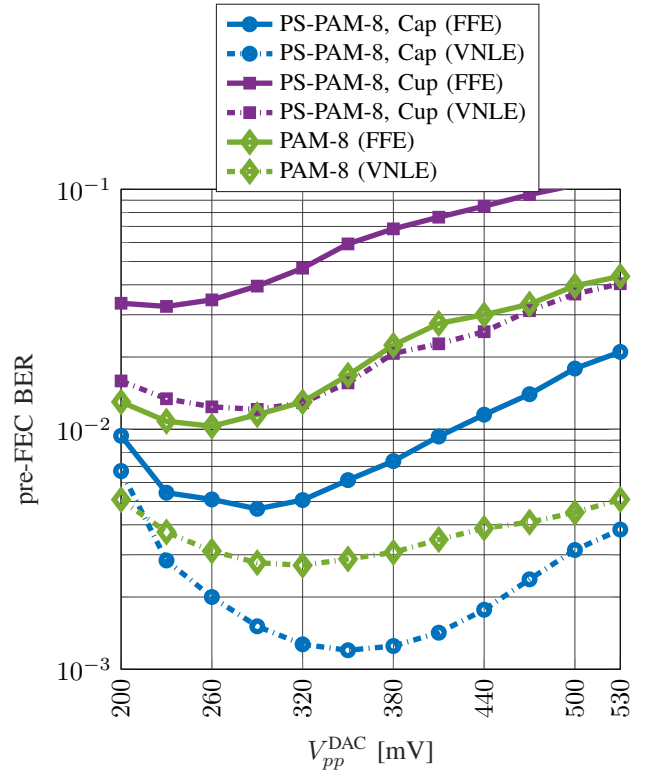


Fig. 5: Driving voltage optimization for uniform and PS PAM-8 with cap and cup-shaped MB distributions (GO 2.0).

in the presence of linear equalization and, at the same time, largely benefit from VNLE.

In summary, uniform PAM-8 is highly susceptible to nonlinear distortion, and cap-shaped PS-PAM-8 with GO 2.0 performs the best, since it allows the highest driving voltage and exhibits the highest nonlinear tolerance. Therefore, we conclude that in the considered scenario, probabilistic constellation shaping with cap-shaped distributions results in nonlinear shaping gain over uniform PAM-8 at the cost of increased symbol rate.

Additionally, while sweeping the driving voltage during V_{pp} optimization, we are deliberately operating both in the linear and nonlinear region of the EML. The left part of the curves in Fig. 5 corresponds to the linear region. If we drive the system in the linear region, we lose performance because of the lower transmit power. From the trend in Fig. 5, it can be extrapolated that the performance gain of PS-PAM-8 with cap shape over uniform PAM-8 will vanish at lower driving voltage.

B. Comparison among Different Gaussian Orders

We have introduced the concept of GO in Eq. 6. Since the cap-shaped MB distribution undoubtedly performs better than the cup-shaped variant, we concentrate our investigation on different GOs on cap-shaped distributions only.

Fig. 7 shows the experimental results for cap-shaped PS-PAM-8 at 110 GBd with PS OH $\approx 8.17\%$ and GO 2.0, 3.5 and 5.0. Similar to the previous investigations, results are presented here in the case of linear and nonlinear equalization. In the case of equalization with linear FFE, for GO 5.0, the optimum V_{pp} is 60 mV higher than for GO 2.0 and

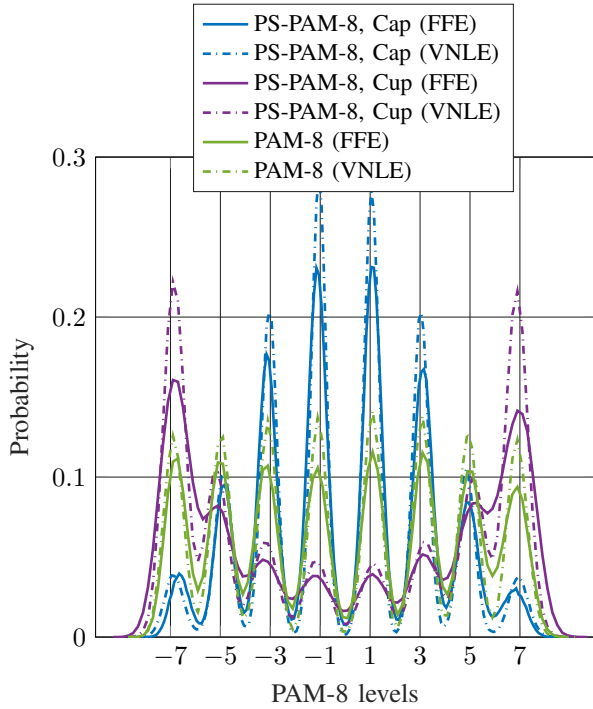


Fig. 6: Histograms of uniform PAM-8 and PS PAM-8 with linear and nonlinear equalization.

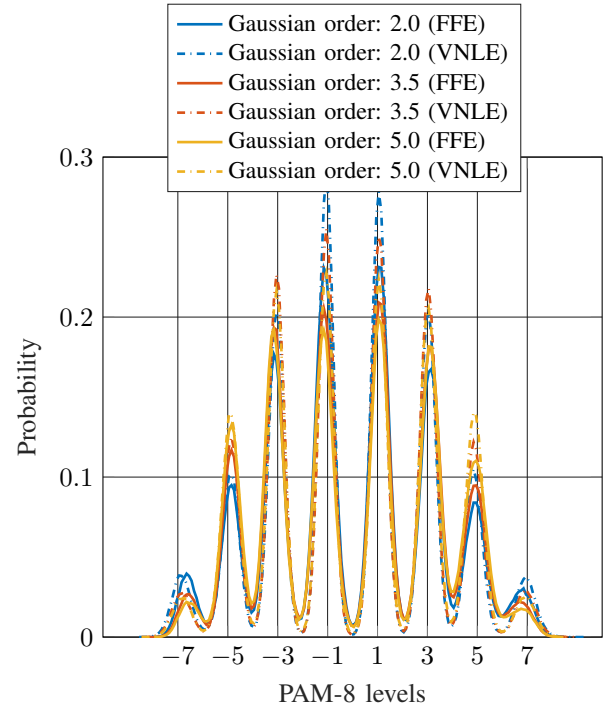


Fig. 8: Signal histograms for cap-shaped distributions of different Gaussian orders with and without nonlinear equalization.

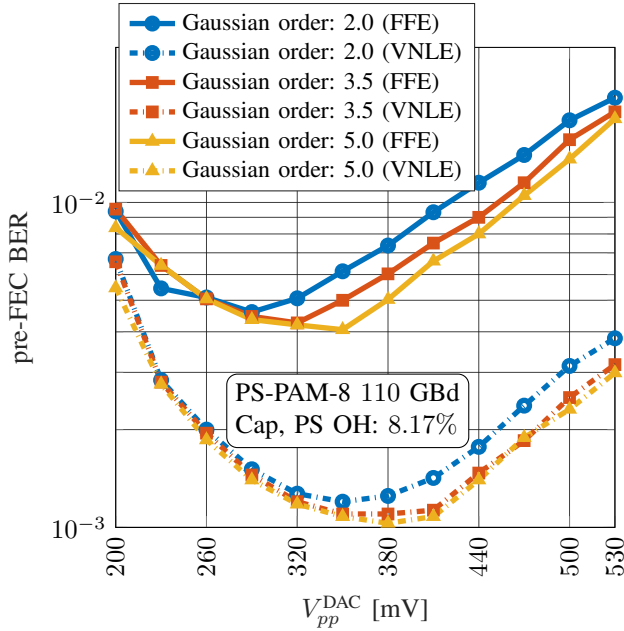


Fig. 7: Driving voltage optimization for cap-shaped distributions of different GOs.

30 mV higher than for GO 3.5. As explained in Section II, the optimum V_{pp} depends on the probability of the symbols mapped on the outer levels. For higher GOs the distribution becomes more compact and a higher V_{pp} can be tolerated. However, in our experiment, the BER improvement due to higher-order GOs is only minor. With VNLE, the optimum driving voltage is increased by 60 mV for all considered GOs and the BER improvement of GO 5.0 compared to GO 2.0 is

marginal. To understand the phenomena, signal histograms for different GOs are presented at their optimum V_{pp} in Fig. 8. In the presence of VNLE, the BER is improved up to 3 times, but the different GOs perform similarly, because, after equalizing the nonlinearity, the main residual impairment is the BW limitation of OE components. Therefore, we can see that going beyond GO 5.0 does not bring significant benefits. Please note that this is different from the scenario considered in [15], where we compared higher-order GOs in the case of less severe bandwidth limitation. In [15] GO 5.0, in term of ROP, performs on average 0.5 to 0.8 dB better compared to GO 2.0. In this scenario [15], we can see that higher GO brings always gain and going beyond GO 5.0 may improve performance further.

Since we assume an HD-FEC, we consider the commonly used pre-FEC BER as performance metric. Note that the AIR for HD is a monotonic function of the BER (computing AIR is described in Sec. V-C). Consequently, optimizing w.r.t. BER or HD-AIR leads to the same optimization outcome.

C. BER, AIR and ONBR vs Symbol Rate

In this section we will concentrate our investigation on uniform PAM-8 and cap-shaped PS-PAM-8 with GO 2.0. Experimental results in terms of pre-FEC BER as a function of the symbol rate are presented in Fig. 9. Considering an HD-FEC with 7% OH (BER threshold of 4.6×10^{-3}) [26], uniform PAM-8 at 100 GBd (red circle (FFE), square (VNLE)) and 110 GBd (red circle FFE, square (VNLE)) is approximately comparable with PS-PAM-8 with PS OH of $\approx 8.17\%$ at 110 GBd (black circle (FFE), square (VNLE)) and 120 GBd

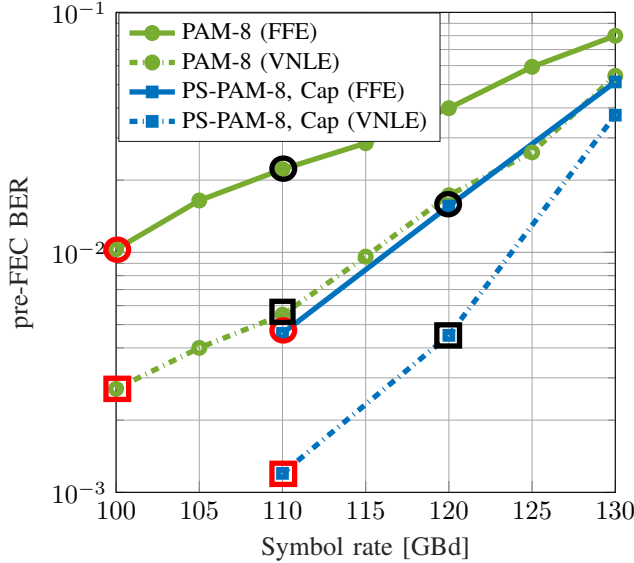


Fig. 9: Experimental comparison of uniform and cap-shaped PS PAM-8.

(black circle (FFE), square (VNLE)), where the NBRs are ≈ 290 Gb/s and ≈ 309 Gb/s, respectively.

Considering equalization with linear FFE only, 110 GBd PS-PAM-8 performs > 5 times better than 100 GBd uniform PAM-8. However, 120 GBd PS-PAM-8 performs only marginally better than 110 GBd uniform PAM-8. The performance of PS-PAM is mainly impaired by the BW limitation of the OE components. VNLE brings gain and, as discussed before, uniform PAM-8 benefits most (more than 7 times) from nonlinear equalization due to its high susceptibility to nonlinearity.

1) *AIR vs Symbol Rate*: In Fig. 10 we present the additional performance metric AIR, which is computed from the BER results (Fig. 9) under the assumption of a binary symmetric channel (BSC). AIR indicates the possible rate of error-free data transmission with capacity-achieving FEC. The AIR for HD is calculated in three steps, following [3, Sec. 8.2.4].

- Step 1: Compute the equivocation under bitwise HD by

$$H_2(p) = -p \cdot \log_2(p) - (1-p) \cdot \log_2(1-p), \quad (8)$$

where H_2 is the binary entropy function and $p = \text{BER}$.

- Step 2: Compute the achievable SE

$$\text{SE}_{\text{HD}} = [\text{H}(X) - m \cdot H_2(\text{BER})]^+, \quad (9)$$

where m is the number of bits per symbol, e.g., $m = 3$ for PAM-8 and $\text{H}(X)$ is the entropy of the input (3 and ≈ 2.77 bits per symbol for uniform and PS PAM-8, respectively).

- Step 3: Compute AIR:

$$\text{AIR} = f_s \cdot \text{SE}_{\text{HD}}, \quad (10)$$

where f_s is the symbol rate.

As shown in Fig. 10, with linear FFE, the highest AIR, which is ≈ 291 Gb/s, is achieved with 110 GBd cap-shaped

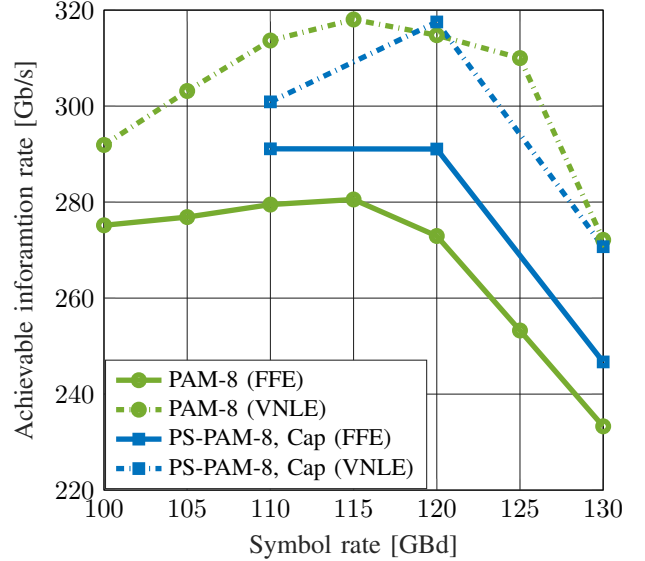


Fig. 10: AIR of uniform and cap-shaped PS PAM-8.

PS-PAM-8, whereas uniform PAM-8 achieves its peak AIR of ≈ 280 Gb/s at 115 GBd. In the presence of VNLE, uniform PAM-8 and PS PAM-8 achieve the same peak AIR of ≈ 318 Gb/s at 115 GBd and 120 GBd, respectively. We emphasize that PS-PAM-8 at 110 GBd with FFE achieves the same performance (≈ 291 Gb/s) of 100 GBd uniform PAM-8 with VNLE in terms of AIR.

2) *ONBR vs Symbol Rate*: As further interpretation of the BER results (Fig. 9), we present in Fig. 11 the net bit rate achieved with a practical FEC code, as a complement to Fig. 10, which assumes capacity-achieving FEC. The ONBR is computed in two steps:

- Step 1: Compute the SE for the modulation formats whose BER lies below the considered threshold (4.6×10^{-3})

$$\text{SE} = [\text{H}(X) - m(1 - R_{\text{FEC}})]^+, \quad (11)$$

where m is the number of bits per symbol, e.g., $m = 3$ for PAM-8, $\text{H}(X)$ is the entropy of the input (3 and ≈ 2.77 bits per symbol for uniform and PS PAM-8, respectively), and R_{FEC} is the considered FEC OH, which is 7%.

- Step 2: Compute ONBR:

$$\text{ONBR} = f_s \cdot \text{SE}, \quad (12)$$

where f_s is the symbol rate.

With linear equalization only PS-PAM-8 (diamond marker) reaches the HD-FEC BER threshold, achieving an ONBR of ≈ 284 Gb/s. On the other hand, with VNLE, both uniform (green dashed line with circle markers) and PS PAM-8 (blue dashed line with square markers) reach the considered BER threshold with peak ONBRs of ≈ 294 Gb/s and ≈ 309 Gb/s, respectively.

VI. CONCLUSION

In this paper, we have discussed PS-PAM-8 for direct-detection systems and introduced a Gaussian order (GO)

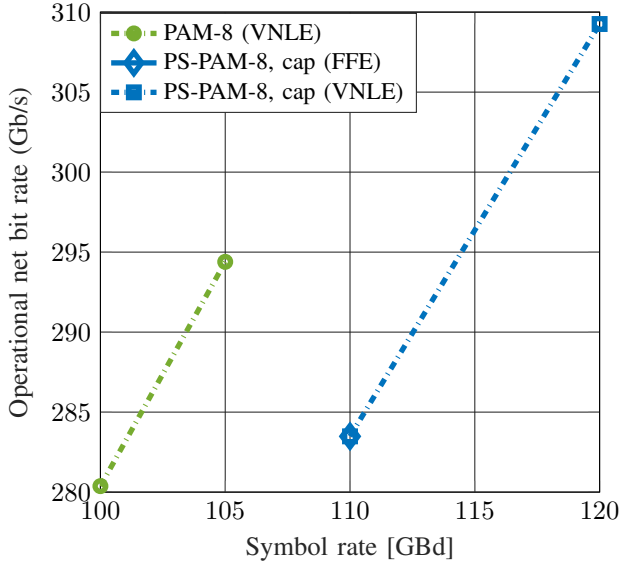


Fig. 11: ONBR of uniform and cap-shaped PS PAM-8.

parameter, which generalizes both the cap and cup-shaped MB distributions.

Cup-shaped distributions are expected to perform well in peak-power constrained (PPC) systems. However, since the transfer function of a practical modulator, e.g. an EML, exhibits a gentle transition from the linear region towards saturation, the considered system, differently from that considered in [16], is not purely PPC. In fact, we find that cap-shaped PS PAM-8 outperforms both uniform PAM-8 and cup-shaped PS PAM-8 by factors > 5 and > 7 in BER with linear equalization, respectively.

A theoretical analysis and a comparison of the signal histograms indicate that cap-shaped probabilistic shaping achieves nonlinear gain at the cost of an increased symbol rate. In detail, a cap-shaped distribution lowers the occurrence probability of the outer signal levels, which are less affected by saturation of the EML transfer curve. This allows an increase of the driving voltage and results in a larger separation between adjacent modulated levels. It is important to observe that the optimization of the driving voltage is fundamental to reveal the nonlinear gain of cap-shaped PAM.

We also investigated modified MB distributions with GOs 3.5 and 5.0 (besides GO 2.0), which further reduce the occurrence of the outer symbols. Although, as expected, a larger GO accommodates a higher driving voltage, the additional BER improvement is marginal due to the severe bandwidth limitation of our experimental setup.

Further, we computed the achievable information rate (AIR) on the binary symmetric channel established between the bit mapper at the transmitter and the hard demapper at the receiver. In the case of linear equalization, on the considered setup, the peak AIR for uniform PAM-8 and PS PAM-8 is ≈ 280 Gb/s and ≈ 291 Gb/s, respectively. In the presence of nonlinear Volterra equalization, the nonlinear PS gain with respect to uniform PAM-8 is reduced, and both modulation formats achieve a similar peak AIR of ≈ 318 Gb/s. Therefore, we

conclude that the use of PS is a low-complexity alternative to power-hungry nonlinear equalization. For example, we observe that 110 GBd PS-PAM-8 with linear equalization reaches the same AIR as 100 GBd uniform PAM-8 with advanced VNLE at the expense of a 10% increase in the symbol rate. Additionally, with practical FEC and linear equalization only cap-shaped PS-PAM-8 achieves an operating net bit rate of ≈ 284 Gb/s.

VII. APPENDIX

An alternative visualization of Fig. 6 is presented in Fig. 12, which shows the level distribution for each PAM-8 symbol after linear FFE and nonlinear VNLE. The overlap among neighboring histograms contributes to the number of symbol errors. For cap-shaped PS PAM-8 with FFE only (Fig. 12 (a)) the overlap is minimized due to the high driving voltage. Conversely, for cup-shaped PS-PAM-8, the limited driving voltage swing results in a massive overlap among neighboring levels. An intermediate scenario is observed for uniform PAM-8. With VNLE the level distributions of all formats are improved with uniform PAM-8 benefiting the most.

REFERENCES

- [1] G. Böcherer, F. Steiner, and P. Schulte, "Bandwidth efficient and rate-matched low-density parity-check coded modulation," *IEEE Transactions on Communications*, vol. 63, no. 12, pp. 4651–4665, 2015.
- [2] P. Schulte, "Algorithms for distribution matching," Ph.D. dissertation, Technical University of Munich, 2020.
- [3] G. Böcherer, "Principles of coded modulation," 2018, habilitation thesis, Technical University of Munich. [Online]. Available: <https://www.georg-boecherer.de/boecherer2018principles.pdf>
- [4] G. Böcherer, P. Schulte, and F. Steiner, "Probabilistic shaping and forward error correction for fiber-optic communication systems," *J. Lightw. Technol.*, vol. 37, no. 2, pp. 230–244, 2019.
- [5] J. Li, A. Zhang, C. Zhang, X. Huo, Q. Yang, J. Wang, J. Wang, W. Qu, Y. Wang, J. Zhang *et al.*, "Field trial of probabilistic-shaping-programmable real-time 200-Gb/s coherent transceivers in an intelligent core optical network," in *Asia Commun. Photonics Conf. (ACP)*, 2018.
- [6] "Nokia Photonic Service Engine 3: Taking light to the limit," Mar. 2018. [Online]. Available: <https://onestore.nokia.com/asset/201772>
- [7] H. Sun, M. Torbatian, M. Karimi, R. Maher, S. Thomson, M. Tehrani, Y. Gao, A. Kumpera, G. Soliman, A. Kakkar *et al.*, "800G DSP ASIC design using probabilistic shaping and digital sub-carrier multiplexing," *J. Lightw. Technol.*, vol. 38, no. 17, pp. 4744–4756, 2020.
- [8] X. Zhou, R. Urata, and H. Liu, "Beyond 1 Tb/s intra-data center interconnect technology: IM-DD or coherent?" *J. Lightw. Technol.*, vol. 38, no. 2, pp. 475–484, 2020.
- [9] J. Cheng, C. Xie, Y. Chen, X. Chen, M. Tang, and S. Fu, "Comparison of coherent and IMDD transceivers for intra datacenter optical interconnects," in *2019 Optical Fiber Communications Conference and Exhibition (OFC)*, 2019, pp. 1–3.
- [10] E. Berikaa, M. S. Alam, and D. V. Plant, "Net 400-Gbps/λ IMDD transmission using a single-DAC DSP-free transmitter and a thin-film lithium niobate MZM," *Opt. Lett.*, vol. 47, no. 23, pp. 6273–6276, Dec 2022. [Online]. Available: <https://opg.optica.org/ol/abstract.cfm?URI=ol-47-23-6273>
- [11] M. S.-B. Hossain, J. Wei, F. Pittalà, N. Stojanović, S. Calabrò, T. Rahman, G. Böcherer, T. Wettlin, C. Xie, M. Kuschnerov, and S. Pachnicke, "402 Gb/s PAM-8 IM/DD O-band EML transmission," in *2021 European Conference on Optical Communication (ECOC)*, 2021, pp. 1–4.
- [12] M. S.-B. Hossain, J. Wei, F. Pittalà, N. Stojanović, S. Calabrò, T. Rahman, T. Wettlin, C. Xie, M. Kuschnerov, and S. Pachnicke, "Single-lane 402 Gb/s PAM-8 IM/DD transmission based on a single dac and an O-band commercial EML," in *26th Optoelectronics and Communications Conference*. Optica Publishing Group, 2021, p. T5A.6. [Online]. Available: <https://opg.optica.org/abstract.cfm?URI=OECC-2021-T5A.6>

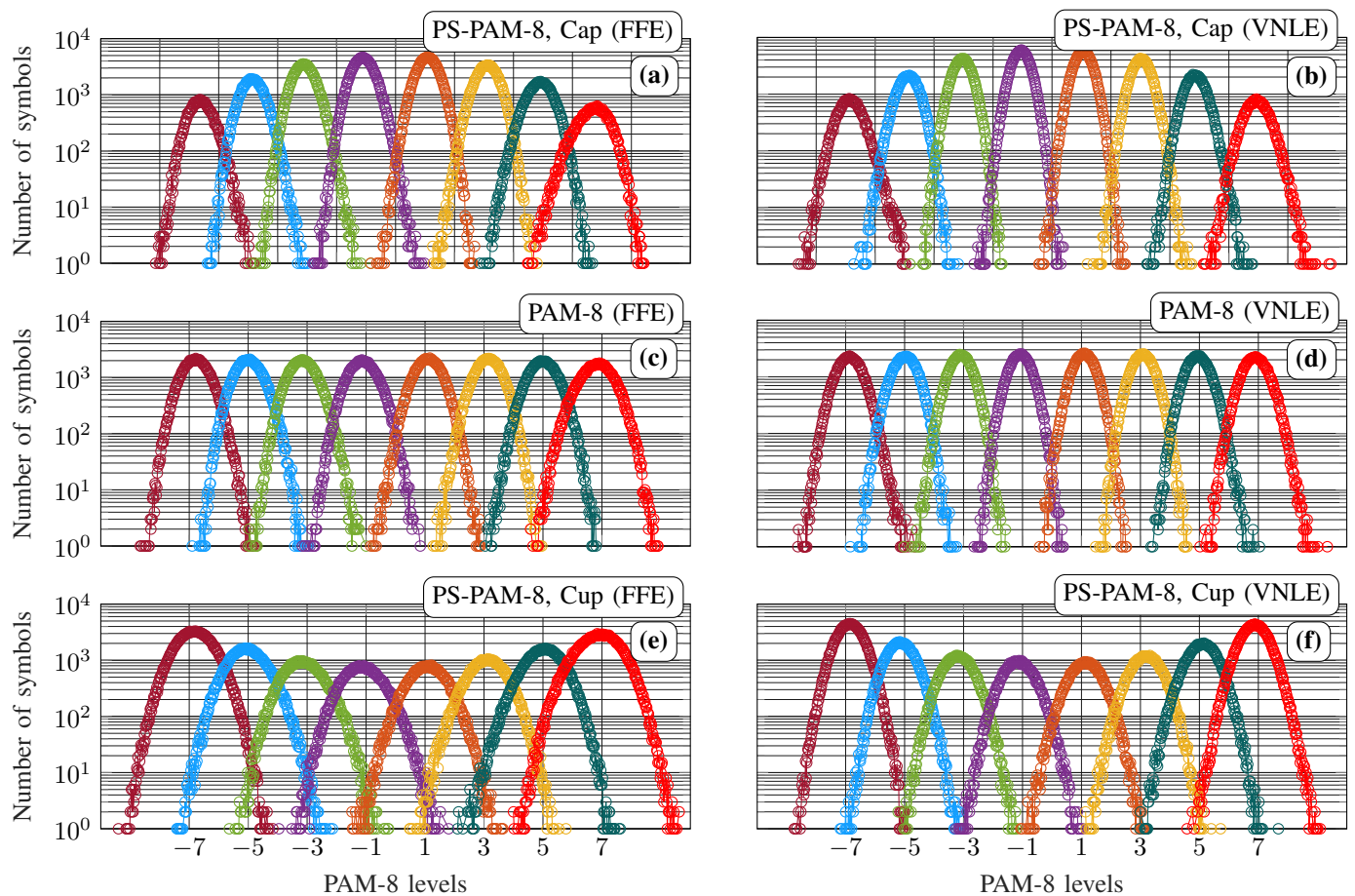


Fig. 12: Level distributions after linear and nonlinear equalization for cap-shaped PS-PAM-8 are shown in (a) and (b), respectively. Similarly, the distributions for uniform PAM-8 and cup-shaped PS-PAM-8 are shown in (c), (d), (e) and (f), respectively.

- [13] M. S.-B. Hossain, T. Rahman, G. Böcherer, N. Stojanović, T. Wettlin, S. Calabrò, J. Wei, C. Xie, and S. Pachnicke, "Experimental comparison of uniform and probabilistically shaped PAM-8 for IM/DD system at transmission rates beyond 200 Gbit/s," in *Optical Fiber Communication Conference (OFC) 2021*. Optica Publishing Group, 2021, p. F2D.6. [Online]. Available: <https://opg.optica.org/abstract.cfm?URI=OFC-2021-F2D.6>
- [14] M. S.-B. Hossain, G. Böcherer, T. Rahman, N. Stojanović, P. Schulte, S. Calabrò, J. Wei, C. Bluemm, T. Wettlin, C. Xie, M. Kuschnerov, and S. Pachnicke, "Experimental comparison of cap and cup probabilistically shaped PAM for O-band IM/DD transmission system," in *2021 European Conference on Optical Communication (ECOC)*, 2021, pp. 1–4.
- [15] M. S.-B. Hossain, G. Böcherer, Y. Lin, S. Li, S. Calabrò, A. Nedelcu, T. Rahman, T. Wettlin, J. Wei, N. Stojanović, C. Xie, M. Kuschnerov, and S. Pachnicke, "Experimental comparison of PAM-8 probabilistic shaping with different Gaussian orders at 200 Gb/s net rate in IM/DD system with O-band TOSA," in *2022 European Conference on Optical Communication (ECOC)*.
- [16] T. Wiegart, F. Da Ros, M. P. Yankov, F. Steiner, S. Gaiarin, and R. D. Wesel, "Probabilistically shaped 4-PAM for short-reach IM/DD links with a peak power constraint," *J. Lightw. Technol.*, vol. 39, no. 2, pp. 400–405, 2021.
- [17] D. Che, J. Cho, and X. Chen, "Does probabilistic constellation shaping benefit IM-DD systems without optical amplifiers?" *J. Lightwave Technol.*, vol. 39, no. 15, pp. 4997–5007, Aug 2021. [Online]. Available: <https://opg.optica.org/jlt/abstract.cfm?URI=jlt-39-15-4997>
- [18] F. Kschischang and S. Pasupathy, "Optimal nonuniform signaling for Gaussian channels," *IEEE Transactions on Information Theory*, vol. 39, no. 3, pp. 913–929, 1993.
- [19] G. Böcherer, "Integration of probabilistic shaping and forward error correction: Spectral efficiency, rate, overhead," in *CNRS/GdR ISIS Workshop on Coding, Modulation, and Signal Processing for Optical Communications, Telecom Paris Tech*, Paris, France, 2019. [Online]. Available: http://www.georg-boecherer.de/boecherer2019integration_slides.pdf
- [20] G. Böcherer, P. Schulte, and F. Steiner, "Probabilistic shaping: A random coding experiment," in *Proc. Int. Zurich Seminar Inf. Commun. (IZS)*, 2020, pp. 12–14.
- [21] T. A. Eriksson, M. Chagnon, F. Buchali, K. Schuh, S. ten Brink, and L. Schmalen, "56 Gbaud probabilistically shaped PAM8 for data center interconnects," in *2017 European Conference on Optical Communication (ECOC)*, 2017, pp. 1–3.
- [22] Z. He, T. Bo, and H. Kim, "Probabilistically shaped coded modulation for IM/DD system," *Opt. Express*, vol. 27, no. 9, pp. 12 126–12 136, Apr 2019. [Online]. Available: <https://opg.optica.org/oe/abstract.cfm?URI=oe-27-9-12126>
- [23] M. N. Tehrani, M. Torbatian, H. Sun, P. Mertz, and K.-T. Wu, "A novel nonlinearity tolerant super-Gaussian distribution for probabilistically shaped modulation," in *2018 European Conference on Optical Communication (ECOC)*, 2018, pp. 1–3.
- [24] K. Zhang, Q. Zhuge, H. Xin, W. Hu, and D. V. Plant, "Performance comparison of DML, EML and MZM in dispersion-unmanaged short reach transmissions with digital signal processing," *Opt. Express*, vol. 26, no. 26, pp. 34 288–34 304, Dec 2018. [Online]. Available: <https://opg.optica.org/oe/abstract.cfm?URI=oe-26-26-34288>
- [25] N. Stojanovic, T. Rahman, S. Calabrò, J. Wei, and C. Xie, "Baud-rate timing phase detector for systems with severe bandwidth limitations," in *2020 Optical Fiber Communications Conference and Exhibition (OFC)*, 2020, pp. 1–3.
- [26] M. Scholten, T. Coe, J. Dillard, and F. Chang, "Implementation of hard-decision FEC for next-generation 40G/100G transmission," in *2009 European Conference on Optical Communication (ECOC)*, vol. WS1.6, 2009. [Online]. Available: https://conference.vde.com/ecoc-2009/programs/documents/ws1_06_mikescholten.pdf